



OPEN

Micro-to-nano-scale deformation mechanisms of a bimodal ultrafine eutectic composite

SUBJECT AREAS:

MATERIALS SCIENCE

MECHANICAL PROPERTIES

Received
3 June 2014Accepted
21 August 2014Published
30 September 2014

Correspondence and requests for materials should be addressed to J.M.P. (jinman_park@hotmail.com) or K.B.K. (kbbkim@sejong.ac.kr)

* These authors contributed equally to this work.

Seoung Wan Lee^{1*}, Jeong Tae Kim^{1*}, Sung Hwan Hong¹, Hae Jin Park¹, Jun-Young Park¹, Nae Sung Lee¹, Yongho Seo², Jin Yoo Suh³, Jürgen Eckert⁴, Do Hyang Kim⁵, Jin Man Park⁶ & Ki Buem Kim¹

¹Hybrid Materials Center (HMC), Faculty of Nanotechnology and Advanced Materials Engineering, Sejong University, 209 Neungdong-ro, Gwangjin-gu, Seoul 143-747, Republic of Korea, ²Graphene Research Institute (GRI) & HMC, Faculty of Nanotechnology and Advanced Materials Engineering, Sejong University, 209 Neungdong-ro, Gwangjin-gu, Seoul 143-747, Republic of Korea, ³High Temperature Energy Materials Research Center, Korea Institute of Science and Technology, Hwarangno 14-gil 5, Seoungbuk-gu, Seoul 136-791, Republic of Korea, ⁴Institute for Complex Materials, IFW Dresden, P.O. Box 27 01 16, D-01171 Dresden, Germany and Institute of Materials Science, TU Dresden, D-01062 Dresden, Germany, ⁵Center for Non-Crystalline Materials, Department of Metallurgical Engineering, Yonsei University, 50 Yonsei-ro, Seodaemun-gu, Seoul 120-749, Republic of Korea, ⁶Global Technology Center (GTC), Samsung Electronics Co., Ltd, 129 Samsung-ro, Yeongtong-gu, Suwon-si, Gyeonggi-do 443-742, Republic of Korea.

The outstanding mechanical properties of bimodal ultrafine eutectic composites (BUECs) containing length scale hierarchy in eutectic structure were demonstrated by using AFM observation of surface topography with quantitative height measurements and were interpreted in light of the details of the deformation mechanisms by three different interface modes. It is possible to develop a novel strain accommodated eutectic structure for triggering three different interface-controlled deformation modes; (I) rotational boundary mode, (II) accumulated interface mode and (III) individual interface mode. A strain accommodated microstructure characterized by the surface topology gives a hint to design a novel ultrafine eutectic alloys with excellent mechanical properties.

The development of ultrafine eutectic composites (UECs) containing micron-scale dendrites in an ultrafine eutectic matrix has been highlighted as a novel strategy to obtain simultaneously high strength and plasticity through controlling the plastic instability during deformation^{1,2}. For example, Ti-based UECs present a superior combination of both a high strength of 1.2 GPa and a plastic strain of more than 10% at room temperature¹. Systematic investigations on the deformation mechanisms of such Ti-based UEC have revealed that the micron-scale dendrites play a dominant role for controlling the strength and plasticity at the early stage of the deformation³. At this stage pronounced interactions of slip bands occur and the deformation is controlled by dislocations that are induced in the micron-scale dendrites⁴. Furthermore, the interaction between slip and shear bands modulates the direction of the slip bands. On the other hand, the ultrafine eutectic matrix of the Ti-based UECs plays a key role to control the behavior at the late stage of deformation by effectively dissipating the localized deformation thus resulting in a rearrangement of the ultrafine eutectic structure along a direction of the primary deformation bands, i.e. primary shear bands⁵. The detailed understanding of the deformation mechanisms that are active in such materials allows to further optimize both the strength and the plasticity of the UECs by manipulating the volume fraction of the micron-scale dendrites and the ultrafine eutectic matrix^{5,6}. However, one of the critical issues in these UECs that still has to be solved is the typical tradeoff between strength and plasticity⁷, i.e. increasing the strength of metallic materials while simultaneously maintaining a large plasticity, such as to generate new high performance materials.

In order to engineer such alloys, the microstructure tailoring of ultrafine eutectic alloys (UEAs) without any micron-scale dendrites and even bimodal ultrafine eutectic composites (BUECs) consisting of two different eutectic structures formed by a pseudo-peritectic reaction have been proposed⁸. Indeed, UEAs and BUECs exhibit homogeneous flow upon deformation without compromising a strength decrease⁹. Microstructural investigations of such UEAs and BUECs have shown that not only structural heterogeneity concerning the length-scale, the morphology and the phase selection in the lamellar structure but also chemical heterogeneity driven by liquid separation of minor elements at the colony boundaries are crucial to achieve plasticity without sacrificing the


Table 1 | Mechanical properties of Al-Cu-Si UECs. Yield strength σ_y , Ultimate fracture strength σ_{max} , Plastic strain ϵ_p , and Constituent phases

Alloys	σ_y (MPa)	σ_{max} (MPa)	ϵ_p (%)	Constituent phases
Al ₇₅ Cu ₁₈ Si ₇	810 ± 20	945 ± 25	1.3 ± 0.5	Al ₂ Cu + Si + Eutectic
Al ₇₆ Cu ₂₂ Si ₂	774 ± 20	777 ± 25	0.2 ± 0.1	Al ₂ Cu + Eutectic
Al ₈₀ Cu ₁₇ Si ₃	750 ± 20	901 ± 25	1.9 ± 0.5	Al ₂ Cu + Bimodal eutectic
Al ₈₀ Cu ₅ Si ₁₅	520 ± 15	698 ± 20	13.7 ± 2	α -Al + Si + Eutectic
Al ₈₁ Cu ₁₃ Si ₆	773 ± 20	1014 ± 25	8 ± 1.5	Bimodal eutectic
Al ₈₃ Cu ₁₁ Si ₆	589 ± 15	735 ± 20	4.6 ± 1	α -Al + Si + Bimodal eutectic
Al ₈₈ Cu ₁₀ Si ₂	518 ± 15	725 ± 20	16.1 ± 2	α -Al + Eutectic

strength¹⁰. Thus, the appropriate selection of minor alloying elements capable to introduce structural and chemical heterogeneity is important to manipulate the ultrafine microstructure in these alloys^{11,12}. Further detailed microstructural investigations on deformed UEAs and BUECs clearly revealed that the homogeneous flow often occurs by effective dissipation of the shear stress along the colony boundaries thus resulting in a rotation of the ultrafine colonies¹³. Meanwhile, the achievable strength of the UEAs and BUECs is governed by the interfaces in the lamellar structure¹⁴. However, so far there have been no attempts to elucidate the microscopic deformation mechanisms of the UEAs and BUECs considering the role of the interfaces in the lamellar structure and of the colony boundaries simultaneously.

Recently, there have been some approaches to elucidate the deformation mechanisms of materials using atomic force microscopy (AFM)¹⁵. Since AFM allows to resolve the topography of deformed specimens from the nano- to the micron-scale, it is possible to reveal the explicit features of slip bands, crack initiation and grain boundary sliding. Based on this view of point, it is believed that the microscopic deformation mechanisms of the UEAs and BUECs can be demonstrated more accurately by using AFM topography images with quantitative height measurement.

From previous investigation of a series of Al-Cu-Si UECs, it is possible to clarify the relationship between phase selection and mechanical properties as listed in Table 1. In general, one can find that the UECs with primary Al₂Cu phase i.e. Al₇₅Cu₁₈Si₇, Al₇₆Cu₂₂Si₂ and Al₈₀Cu₁₇Si₃ alloys present a relative high strength with limit plasticity. On the other hand, the UECs with primary α -Al phase i.e. Al₈₀Cu₅Si₁₅, Al₈₃Cu₁₁Si₆ and Al₈₈Cu₁₀Si₂ alloys show high deformability with low strength at room temperature. However, it is worth to note that Al₈₁Cu₁₃Si₆ BUEC reveals high strength without significant compromising plasticity. It is believed that the BUEC with different length-scale of eutectic structure is considered to have desirable microstructure to optimize the strength and plasticity together. Furthermore, it is necessary to elucidate the deformation mechanism of the BUEC to clearly understand the roles of the heterogeneities leading both high strength and large plasticity during deformation. Thus, we have chosen the Al₈₁Cu₁₃Si₆ BUEC as a typical example to clearly understand the microscopic deformation mechanism by measuring the nano- to micro-scale topographical change using AFM.

Figure 1 shows the XRD pattern and a SEM backscattering electron (BSE) micrograph together with a TEM bright-field image of the as-cast Al₈₁Cu₁₃Si₆ alloy. The sharp diffraction peaks in Fig. 1a were identified as a mixture of a face-centered cubic (f.c.c.) α -Al solid solution (Fm3m, $a = 0.4049$ nm), a body-centered tetragonal (b.c.t.) θ phase (Al₂Cu) (I4/mcm, $a = 0.6063$ nm and $c = 0.4872$ nm) and a diamond cubic (d.c.) Si phase (Fd3m, $a = 0.5430$ nm). The BSE micrograph in Fig. 1b reveals the formation of a typical bimodal ultrafine eutectic structure. Coarse and fine eutectic structures with different length-scale of lamellar spacing coexist, as marked by the arrows in Fig. 1b. The volume fraction of the coarse eutectic colonies was measured to be 70–80 vol.%

throughout the sample. The coarse eutectic structures with an average size (i.e. colony size) of 5–10 μm are homogeneously embedded in a fine eutectic matrix implying that the coarse eutectic colonies form first upon solidification.

The TEM micrograph in Fig. 1c reveals that the coarse eutectic structure consists of a mixture of α -Al and θ -Al₂Cu phases. The length-scale of the lamellae in the coarse eutectic is 100–200 nm. On the contrary, the fine eutectic matrix consisting of a mixture of α -Al, θ -Al₂Cu and Si phases has a typical anomalous ternary eutectic structure. The EDX results indicate that only the fine eutectic matrix contains a high amount of Si implying that there is no chance to form a Si phase in the coarse eutectic colonies. The quantitative chemical analysis of the primary coarse eutectic colony and fine eutectic matrix shows that there are 96.80 ± 0.5 at.% Al, 2.65 ± 0.05 at.% Cu and 0.55 ± 0.02 at.% Si in the α -Al phase, 63.78 ± 0.3 at.% Al, 35.37 ± 0.2 at.% Cu and 0.85 ± 0.05 at.% Si in the θ -Al₂Cu phase (for coarse eutectic) and 96.33 ± 0.5 at.% Al, 2.71 ± 0.05 at.% Cu and 0.96 ± 0.02 at.% Si in the α -Al phase, 61.34 ± 0.3 at.% Al, 36.75 ± 0.2 at.% Cu and 1.91 ± 0.05 at.% Si in the θ -Al₂Cu phase and 10.33 ± 0.1 at.% Al, 6.53 ± 0.05 at.% Cu and 83.14 ± 0.5 at.% Si in the Si phase (for fine eutectic matrix), respectively. This reveals that partitioning of Si has a significant influence to primarily form the coarse eutectic structure with a typical lamellar structure, stabilized by the topological and crystallographic anisotropy of the α -Al and θ -Al₂Cu phases upon solidification^{16,17}. Figure 1d displays a typical room temperature engineering stress-strain curve of the as-cast Al₈₁Cu₁₃Si₆ BUEC under tensile testing. The yield strength, σ_y , fracture strength, σ_f and plastic strain, ϵ_p , are 538 MPa, 708 MPa and 3.3%, respectively. The inset SEM micrograph in Fig. 1d obtained from the fracture surface of the alloy clearly reveals the formation of equiaxed dimples with a “cup-like” concave contour as indicated by arrows. Moreover, the size of the dimple areas of 5–10 μm is more or less of same size as the coarse eutectic colonies shown in Fig. 1b. From previous investigations on the microscopic deformation mechanism of UEAs and BUECs^{8,17}, it is known that the dimples on the fracture surface are a result of the rotation of the eutectic colonies with length-scale heterogeneity along the boundaries of the spherical eutectic colonies. Such rotational motion of the eutectic colonies often accompanies complex plastic flow features such as wavy flow patterns to effectively dissipate the localization of the shear stress during deformation¹⁸.

The SEM micrograph in Figure 2a obtained from the lateral surface of the fractured sample shows localized shear deformation bands. Figure 2b clearly reveals a characteristic wavy pattern of the shear bands along the primary colony boundary suggesting an effective dissipation of the localization of the shear stress. The length-scale of the wavy pattern of the shear band is approximately 7 μm , as indicated in Fig. 2b. This oscillation-length of the wavy propagation of the shear bands is more or less identical to the length-scale of the shear bands as well as the colony size, i.e. 5–10 μm , as shown in Fig. 1b. This suggests that the propagation of shear bands along the interface of the primary eutectic colonies is possibly caused by a rotational mechanism of the eutectic colony, similarly to previous

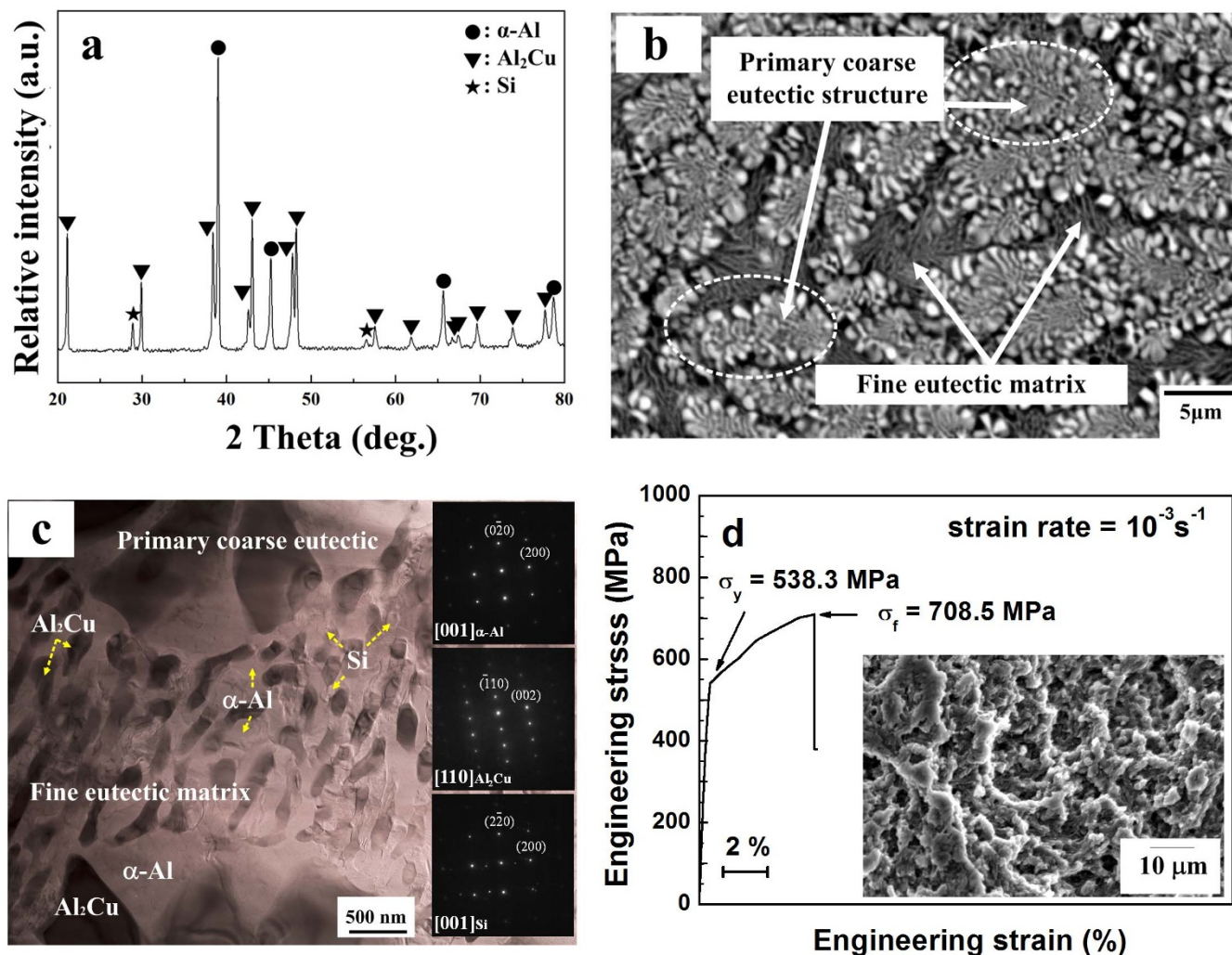


Figure 1 | Phase, microstructural analyses and mechanical properties. (a), XRD pattern. (b), BSE SEM image. (c), BF TEM image. (d), tensile stress-strain curve of the as-cast $\text{Al}_{81}\text{Cu}_{13}\text{Si}_6$ bulk ultrafine eutectic composite. The insets in (c) and (d) show the SAED patterns obtained from the as-cast sample and the SEM micrograph obtained from the fractured sample, respectively.

investigations on the deformation behavior of Ti-, Fe- and Mg-based BUECs^{9,19,20}. The AFM images obtained from the same area shown in Figs. 2c and d reveal that both the length-scale and the oscillation-length of the wavy propagation of the shear bands are $\sim 7 \mu\text{m}$. This clearly shows that the interfaces between the primary eutectic structure and the matrix, i.e. the colony boundaries, play an important role to effectively accommodate the shear strain. As suggested by previous investigations on the deformation behavior of BUECs⁹, the rotation of the primary eutectic colonies allows to effectively dissipate the excessive stress concentration that otherwise would cause localization of the shear stress during deformation. Based on this understanding, it is possible to suggest that the interfaces of the ultrafine structure in the primary eutectic colonies have a similar influence for controlling the deformation behavior of the BUECs.

In order to elucidate the effect of the interfaces of the ultrafine lamellar structure in the primary colonies, it is necessary to determine the detailed change of the height profile using AFM. Figure 3a displays a typical cross-sectional height profile of the lateral surface of a fractured sample along the white dot line of $\sim 30 \mu\text{m}$ shown in Fig. 2c. As indicated by the dotted lines in Fig. 3a, there is a typical unit distance of $5 \sim 10 \mu\text{m}$ determined by a sudden drop of the height by $200 \sim 250 \text{ nm}$. This typical unit distance appears regularly and is identical to the size of the primary eutectic colonies of $5\text{--}10 \mu\text{m}$, as shown in Figs. 1b and 2a. This finding suggests that the

significant change in the height is possibly caused by the accommodation of the localized shear strain at the boundary of the primary colonies during deformation. The schematic drawing in Fig. 3a illustrates that the regular occurrence of the distinct change of the height by $200 \sim 250 \text{ nm}$ in depth at the primary colony boundaries can be linked to the rotation of the primary colony boundaries in order to accommodate the strain. Macroscopically, the rotation of the primary colonies contributes to the plasticity of the sample through the so-called rotational boundary mode^{9,13}.

When inspecting the deformation mechanisms of the $\text{Al}_{81}\text{Cu}_{13}\text{Si}_6$ BUEC more closely, one can find several small stepped-height changes within the regular unit length suggesting that microscopic and mesoscopic deformation occurs in the primary eutectic colony. Fig. 3b displays a detailed AFM height profile obtained from the fracture surface of a primary eutectic colony with a size of $\sim 10 \mu\text{m}$, which is identical to the regular unit distance as described in Fig. 3a. In general, it is possible to categorize the height changes into two distinct features along the lateral distance, as indicated by i) and ii) as marked in Fig. 3b. In general, the point i) often contains typical nano-scale height steps with $5 \sim 20 \text{ nm}$ in depth. These nano-scale height steps usually occur through the height profile and are more or less identical to the length-scale of the lamellar spacing ($100 \sim 200 \text{ nm}$) in the primary eutectic colonies, as determined by TEM (Fig. 1c). This reflects that the interfaces of the lamel-

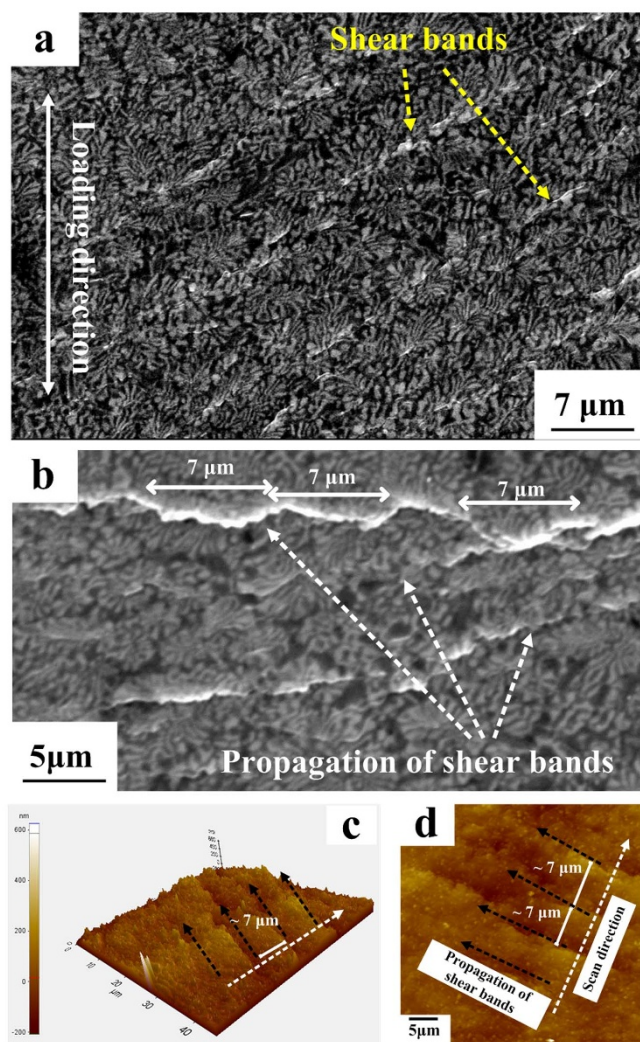


Figure 2 | Lateral and fracture surface morphologies. (a–b), BSE SEM image, (c–d), AFM morphologies of lateral surface after tensile testing.

lar structure in the primary eutectic colonies also effectively accommodate the local deformation strain during deformation. Thus, not only the interfaces of the primary colony boundaries (i.e. rotation of the colony boundaries), but also the interfaces of the lamellar structure in the primary eutectic colonies are important to efficiently accommodate the strain. Furthermore the point ii) corresponds to typical height steps of 80–90 nm in depth. This height change occurs by the accumulation of three or four lamellar structures in the primary colony. From the AFM height profile measurements, one can infer the details of the deformation mechanisms of $\text{Al}_{81}\text{Cu}_{13}\text{Si}_6$ BUEC by the schematic illustration sketched in Fig. 3c indicating three different modes: (I) rotational boundary mode, (II) accumulated interface mode and (III) individual interface mode. However, the interfaces of either the colony boundary or the lamellar structure have a significant difference concerning the ability to accommodate the strain because of their different characteristics in terms of structural coherency^{21–24}. In other words, depending on the degree of lattice mismatch among the matrix, colony boundaries and individual eutectic interfaces stress relaxation and strain accommodation capacities can be significantly altered. Such a distinct lattice mismatch of interfaces/boundaries causes the spatial heterogeneous strain distribution and different strain relaxation behavior during deformation^{25–27}. The rotational boundary mode (I) occurs at the colony boundaries between the primary and matrix eutectic structures. Due to high height change determined from the AFM height

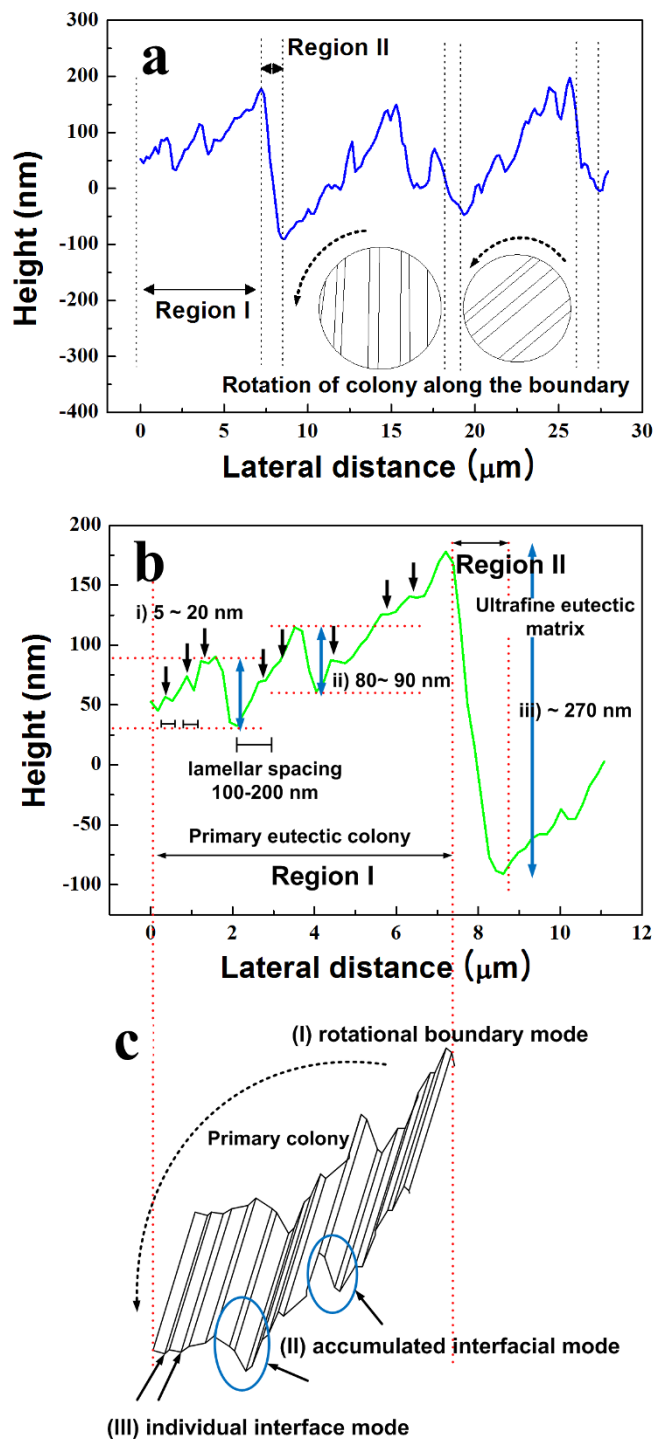


Figure 3 | Deformation mechanism under tensile load. (a–b), Height profiles of shear bands along the lateral surface. (c), Schematic illustration of the deformation behavior of the as-cast $\text{Al}_{81}\text{Cu}_{13}\text{Si}_6$ bulk ultrafine eutectic composite during tensile deformation.

profiles, it is believed that the rotational interface mode at the colony boundaries has a dominant effect to accommodate the strain during the deformation of the $\text{Al}_{81}\text{Cu}_{13}\text{Si}_6$ BUEC. The accumulated interface mode (II) is considered as an unique way to accommodate the strain inside the primary colonies. Compared to the individual interface mode (III), the amount of strain accommodation is relatively high as inferred from the height change. Altogether, our findings suggest that the reason to activate the accumulated interface mode is due to the need to release the stress concentration at the interfaces



of the lamellar structure. Apparently, the individual interface mode (III) originating from the coherent interfaces in the primary colonies can gradually destroy the structural coherency during deformation. Hence, the combination of the accumulated interface mode (II) and the individual interface mode (III) allows accommodating a considerable amount of plastic strain for the ultrafine eutectic structure.

As described above, it is possible to develop a novel strain accommodated eutectic structure through triggering three different interface-controlled deformation modes; (I) rotational boundary mode, (II) accumulated interface mode and (III) individual interface mode. Especially, the unique accumulated interface mode plays an important role to release the stress concentration at the interfaces of the lamellar structure which is operated by the individual interface mode (III). It is obvious that the rotational interface mode at the primary colony boundaries has a dominant effect to accommodate the strain. Of course, there is no doubt that further investigations are necessary to fully interpret the high strength and plasticity of the BUECs in light of the details of the deformation mechanisms governed by the three different interface modes. Nevertheless, this novel finding of a strain accommodated eutectic structure can give valuable information to design superior ultrafine eutectic alloys with excellent mechanical properties.

Methods

The $\text{Al}_{81}\text{Cu}_{13}\text{Si}_6$ alloy used for the present study was prepared by arc melting pure elements (purity > 99.8%) under an argon atmosphere¹⁵. A master alloy ingot was remelted at least four times to guarantee compositional homogeneity. From this master alloy cylindrical rod-shape samples of 3 mm diameter and 50 mm length were fabricated using a suction casting facility. The phases present in the alloy were identified by X-ray diffraction (XRD, Rigaku-D/MAX-2500/PC) with $\text{Cu K}\alpha_1$ radiation ($\lambda = 1.5406 \text{ \AA}$). Scanning electron microscopy (SEM: JEOL JSM-6390) combined with energy-dispersive spectrometry (EDX) was employed for microstructure observation and composition analysis. A transmission electron microscope (TEM, Tecnai F20) was used for structural characterization. Thin foil samples for TEM analysis were prepared by conventional ion milling (Gatan, Model 600). The mechanical properties were evaluated under uniaxial tension loading with an initial strain rate of $1 \times 10^{-3} \text{ s}^{-1}$ at room temperature (Shimazu Universal Tester). For tensile testing, the samples were machined and polished into dog-bone-shaped specimens with a gauge length of 10 mm and a cross section of $2 \text{ mm} \times 1 \text{ mm}$. Systematic studies of the lateral surfaces of the fractured sample were done in order to clarify the microscopic deformation modes using non-contact mode atomic force microscopy (PSIA, South Korea) with a standard pyramidal tip having a radius of curvature of less than 50 nm.

1. He, G., Eckert, J., Löser, W. & Schultz, L. Novel Ti-base nanostructure–dendrite composite with enhanced plasticity. *Nat. Mater.* **2**, 33–37 (2003).
2. Park, J. M. *et al.* Nanostructure–dendrite composites in the Fe–Zr binary alloy system exhibiting high strength and plasticity. *Scripta Mater.* **57**, 1153–1156 (2007).
3. Louzguine, D. V., Louzguina, L. V., Kato, H. & Inoue, A. Investigation of Ti–Fe–Co bulk alloys with high strength and enhanced ductility. *Acta Mater.* **53**, 2009–2017 (2005).
4. Kim, K. B., Das, J., Xu, W., Zhang, Z. F. & Eckert, J. Microscopic deformation mechanism of a $\text{Ti}_{66.1}\text{Nb}_{13.9}\text{Ni}_{4.8}\text{Cu}_8\text{Sn}_{7.2}$ nanostructure–dendrite composite. *Acta Mater.* **54**, 3701–3711 (2006).
5. Ma, E. Nanocrystalline materials: Controlling plastic instability. *Nat. Mater.* **2**, 7–8 (2003).
6. Park, J. M. *et al.* Propagation of shear bands and accommodation of shear strain in the $\text{Fe}_{56}\text{Nb}_4\text{Al}_{40}$ ultrafine eutectic–dendrite composite. *Appl. Phys. Lett.* **92**, 091910–3 (2008).
7. Park, J. M. *et al.* Multi-phase Al-based ultrafine composite with multi-scale microstructure. *Intermetallics* **10**, 1829–1833 (2010).
8. Song, G. A. *et al.* Heterogeneous eutectic structure in Ti–Fe–Sn alloys. *Intermetallics* **19**, 536–540 (2011).
9. Park, J. M., Kim, D. H., Kim, K. B. & Kim, W. T. Deformation-induced rotational eutectic colonies containing length-scale heterogeneity in an ultrafine eutectic $\text{Fe}_{83}\text{Ti}_7\text{Zr}_6\text{B}_4$ alloy. *Appl. Phys. Lett.* **91**, 131907–3 (2007).

10. Liddicoat, P. V. *et al.* Nanostructural hierarchy increases the strength of aluminium alloys. *Nat. Commun.* **1**, 63–7 (2010).
11. Park, J. M., Kim, D. H., Kim, K. B. & Eckert, J. Improving the plasticity of a high strength Fe–Si–Ti ultrafine composite by introduction of an immiscible element. *Appl. Phys. Lett.* **97**, 251915–3 (2010).
12. Kim, K. H., Ahn, J. P., Lee, J. H. & Lee, J. C. High-strength Cu–Zr binary alloy with an ultrafine eutectic microstructure. *J. Mater. Res.* **23**, 1987–1994 (2008).
13. Das, J., Kim, K. B., Baier, F., Löser, W. & Eckert, J. High-strength Ti-base ultrafine eutectic with enhanced ductility. *Appl. Phys. Lett.* **87**, 161907–3 (2005).
14. Patricia, B. O. *et al.* Ultra-high-strength nanofibrillar Al_2O_3 –YAG–YSZ eutectics. *Adv. Mater.* **19**, 2313–2318 (2007).
15. Kim, J. J., Choi, Y., Surech, S. & Argon, A. S. Nanocrystallization during nanoindentation of a bulk amorphous metal alloy at room temperature. *Science* **295**, 654–657 (2002).
16. Park, J. M. *et al.* High-strength bulk Al-based bimodal ultrafine eutectic composite with enhanced plasticity. *J. Mater. Res.* **24**, 2605–2609 (2009).
17. Park, J. M. *et al.* Microstructural modulations enhance the mechanical properties in Al–Cu–(Si, Ga) ultrafine composites. *Adv. Eng. Mater.* **12**, 1137–1141 (2010).
18. Kim, K. B. *et al.* Propagation of shear bands in a $\text{Cu}_{47.5}\text{Zr}_{47.5}\text{Al}_5$ bulk metallic glass. *J. Mater. Res.* **23**, 6–12 (2008).
19. Louzguine, D. V., Louzguina, L. V., Polkin, V. I. & Inoue, A. Deformation-induced transformations in $\text{Ti}_{60}\text{Fe}_{20}\text{Co}_{20}$ alloy. *Scripta Mater.* **57**, 445–448 (2007).
20. Shi, L. L., Xu, J. & Ma, E. Mg–Al–Ca in-situ composites with a refined eutectic structure and their compressive properties. *Metall. Mater. Trans. A* **39**, 1225–1235 (2008).
21. Greer, J. R. Nanotwinned metals: It's all about imperfections. *Nat. Mater.* **12**, 689–690 (2013).
22. Gleiter, H. Nanostructured Materials. *Adv. Mater.* **4**, 474–481 (1992).
23. Wang, Y. M. *et al.* Defective twin boundaries in nanotwinned metals. *Nat. Mater.* **12**, 697–702 (2013).
24. Liu, G. *et al.* Nanostructured high-strength molybdenum alloys with unprecedented tensile ductility. *Nat. Mater.* **12**, 344–350 (2013).
25. Valiev, R. Z. Nanostructured alloys: large tensile elongation. *Nat. Mater.* **12**, 289–291 (2013).
26. Wang, Y. M., Chen, M., Zhou, F. & Ma, E. High tensile ductility in a nanostructured metal. *Nature* **419**, 912–915 (2002).
27. Zhao, Y. H., Liao, X. Z., Cheng, S., Ma, E. & Zhu, Y. T. Simultaneously increasing the ductility and strength of nanostructured alloys. *Adv. Mater.* **18**, 2280–2283 (2006).

Acknowledgments

This work was supported by the Global Research Laboratory (GRL) and the National Research Foundation of Korea (NRF) grant (No. 2013R1A2A2A05006550). One of the authors, Y. Seo, specially thanks to the support from Priority Research Centers Program through the National Research Foundation of Korea (NRF) (No. 2010-0020207).

Author contributions

S.W.L., J.T.K., S.H.H., H.J.P., J.-Y.P., N.S.L. and Y.S. fabricated the ultrafine composite and analyzed their properties; J.-Y.S. carried out the microscopy experiments; S.W.L., J.T.K., J.M.P. and K.B.K. designed the experiments and analyzed the experimental results; J.E., D.H.K., J.M.P. and K.B.K. wrote the paper. All authors discussed and commented on the manuscript.

Additional information

Competing financial interests: The authors declare no competing financial interests.

How to cite this article: Lee, S.W. *et al.* Micro-to-nano-scale deformation mechanisms of a bimodal ultrafine eutectic composite. *Sci. Rep.* **4**, 6500; DOI:10.1038/srep06500 (2014).



This work is licensed under a Creative Commons Attribution-NonCommercial-NoDerivs 4.0 International License. The images or other third party material in this article are included in the article's Creative Commons license, unless indicated otherwise in the credit line; if the material is not included under the Creative Commons license, users will need to obtain permission from the license holder in order to reproduce the material. To view a copy of this license, visit <http://creativecommons.org/licenses/by-nc-nd/4.0/>